Journal of Membrane Science 603 (2020) 118012

Contents lists available at ScienceDirect

Journal of Membrane Science

journal homepage: http://www.elsevier.com/locate/memsci

Determination of parvovirus retention profiles in virus filter membranes using laser scanning microscopy

Remo Leisi [a,*], Jan Bieri [a], Nathan J. Roth [b], Carlos Ros [a]

[a] Department of Chemistry and Biochemistry, University of Bern, Freiestrasse 3, 3012, Bern, Switzerland
[b] CSL Behring AG, Wankdorfstrasse 10, 3000, Bern 22, Switzerland

ARTICLE INFO

Keywords:
Virus filtration
Nanofiltration
Filter membrane
Parvovirus retention profile
Laser scanning microscopy

ABSTRACT

Virus filtration is a highly effective method in the downstream processing of biotherapeutic products to provide effective removal of potential infectious agents based on a size exclusion mechanism. The direct visualization of viruses retained inside the filter membrane represents a valuable tool to get a deeper understanding of the filtration process and to explain observations of virus breakthrough under particular operating conditions. Parvoviruses, which are used as worst-case models in validation studies, were purified and labeled with fluorescent dyes to detect their retention pattern inside the filter membrane using laser scanning microscopy. Critical factors influencing the reproducibility and accuracy of the approach were identified and optimized. The retention profiles revealed detectable differences between viruses, suggesting that the use of bacteriophages or nanoparticles as surrogates is limited in their applicability to accurately predict the behavior of parvoviruses in filter membranes. The established method enables a direct and quantitative analysis of the virus retention profile, adding a valuable tool to the conventional measurement of the viral load reduction to better understand the mechanism underlying the removal of viruses during nanofiltration of biotherapeutic products.

1. Introduction

The production of biotherapeutics relies on biological resources such as cultured cells or donated blood plasma, which carry the inherent risk to be contaminated with viral agents. Mammalian cells used for the production of recombinant proteins such as monoclonal antibodies are known to spontaneously express endogenous retrovirus-like particles [1]. Adventitious contaminations of viruses on the other hand can be introduced into the cell culture by raw materials. In the case of plasma-derived biotherapeutics, the risk involves plasma-borne viruses that may potentially enter the manufacturing process despite the systematic monitoring of donors and screening of the donations. Therefore, the manufacture of biotherapeutic products includes dedicated process steps to inactivate or remove potential viral contaminants. Inactivation of viruses can be achieved by established methods such as low pH, solvent/detergent or heat treatment [2,3]. However, the efficacy and applicability of these treatments depend on the virus and the therapeutic molecule, respectively [4].

Nanofiltration retains viral capsids on a size-based sieving mechanism and is the most robust and effective downstream method to achieve viral clearance [5]. Virus filter membranes consist of hydrophilized polymers like poly(vinylidene fluoride) (PVDF), polyethersulfone (PES) or regenerated cellulose (RC) [3], constituting a complex network of voids and capillaries with a nominal pore size significantly smaller than most viruses.

Parvoviruses are considered the smallest potential viral contaminants that may be present in the manufacture of biological products. The rodent parvovirus minute virus of mice (MVM) has repeatedly caused contaminations of bioreactors for recombinant protein expression due to its ability to replicate in the commonly used Chinese hamster ovarian (CHO) cells [6,7]. Human parvovirus B19 (B19V), which establishes high-level viremia and shows a high prevalence worldwide [8], represents a relevant risk to plasma-derived medicinal products. Parvovirus-grade filter membranes typically have a nominal pore size around 18–20 nm, which is smaller than the outer capsid diameter of parvoviruses (27–28 nm) [9–11], but larger than biotherapeutic products like immunoglobulins isotype G (IgG) (10–12 nm) [12,13]. Due to their small size and high stability against physicochemical inactivation, parvoviruses such as canine parvovirus (CPV), porcine parvovirus (PPV) or MVM represent the worst-case virus challenge in validation studies to demonstrate viral clearance [14,15].

Virus filtration studies are commonly based on measurements of the viral load reduction between feed and filtrate and expressed as the

* Corresponding author.
E-mail address: remo.leisi@dcb.unibe.ch (R. Leisi).

https://doi.org/10.1016/j.memsci.2020.118012
Received 10 December 2019; Received in revised form 30 January 2020; Accepted 29 February 2020
Available online 5 March 2020

Abbreviations

AEX	anion exchange chromatography
AGE	agarose gel electrophoresis
CHO	Chinese hamster ovarian cells
CPV	canine parvovirus
dpi	days post-infection
DLS	dynamic light scattering
DOL	degree of labeling
EM	electron microscopy
HRP	horse-radish peroxidase
LSM	laser scanning microscopy
LRV	logarithmic reduction value
MALDI-TOF	matrix-assisted laser desorption/ionization-time-of-flight
MVM	minute virus of mice
NHS-Atto	N-hydroxy-succinimide ester-modified Atto dye
qPCR	quantitative polymerase chain reaction
PBS	phosphate-buffered saline
PPV	porcine parvovirus
PVDF	poly(vinylidene fluoride)
SDS-PAGE	sodium dodecyl sulfate polyacrylamide gel electrophoresis
TEM	transmission electron microscopy
VLP	virus-like particle

logarithmic reduction value (LRV) of the virus titer. The LRV provides a reliable information regarding the removal of the infectious virus and hence is used to validate the pathogen safety of biotherapeutics. However, the measurement of the LRV relies on the detection of a very small proportion of viruses in the filtrate (<0.01%), while the great majority of the viral particles are retained in the filter (>99.99%) and remain undetectable with this method. Therefore, the LRV alone can only provide partial information about the mechanism of retention of viruses in the membrane. To better understand the mechanisms underlying virus retention, there is a need to obtain a more complete picture of the nanofiltration process.

Different approaches have been reported to visualize the retained particles inside the filter membrane. This can most conveniently be achieved by means of artificial nanoparticles, like gold particles [16–18] or fluorescently labeled nanospheres [19], which have a defined average size and are easily detected in the filter membrane either by electron microscopy (EM) or by fluorescence microscopy. In recent studies, gold nanoparticles and EM have been employed to analyze the correlation between the pore size distribution and virus breakthrough [20], and to understand the phenomenon of membrane fouling [21].

Other studies used laser scanning microscopy (LSM) to detect fluorescently labeled bacteriophages in the filter membrane [22,23]. This technique allows a fast and reproducible visualization of the particle retention patterns independently from other proteins in the feedstream and offers the possibility for co-spiking in the same filtration experiment by means of different fluorescent dyes. This method fundamentally helped to understand viral breakthrough during depressurization events and particle retention during membrane fouling [24,25]. Small bacteriophages such as PP7, MS2 or ΦX174 are used as surrogates in filter research and development, as they have a similar size as parvoviruses, but can more easily be propagated in prokaryotic cell cultures, thus facilitating the virus preparation and detection. Nevertheless, studies based on bacteriophages remain a research tool and are not accepted for regulatory submissions. To ensure the robustness of the virus filtration step with a realistic contaminant, the use of parvoviruses is required [26].

Direct visualization of nanoparticles and bacteriophages is very useful to improve the understanding of the retention mechanism of small particles in the parvovirus-grade filter membranes, but it remains unknown whether these model particles appropriately reflect the behavior of parvoviruses during filtration and whether they can accurately predict the critical separation-active layer in the membrane. Different previous studies have demonstrated that the retention of small viruses, which have a diameter close to the nominal pore size of the filter, is not only determined by size, but also depends on interactions of the capsid surface with the membrane or the biotherapeutic product. These interactions are characteristic for a particular virus, filter membrane, filtration conditions and specific product used [27–29]. In line with this, significant differences in breakthrough were detected between the related parvoviruses MVM and CPV in two different product feedstreams [15]. Interestingly, the differences observed were also influenced by the filtration conditions and material of the filter membrane. Taken together, these studies conclude that each product and process condition need to be evaluated on a case-by-case basis and that in this context even parvovirus models cannot be interchangeably used.

However, studies to get an accurate and deep understanding of the retention mechanism of parvoviruses have been limited, which is mainly attributed to the challenge to obtain sufficient amounts of pure virus stocks. In the past decade, only a few studies achieved to visualize the retention of parvoviruses in filters using transmission electron microscopy (TEM) and immunodetection of B19V [17,30] or PPV [31]. The detection of viral particles by TEM represents an interesting research tool, but is not a practical method to determine virus retention profiles representative for manufacturing conditions.

Previous virus filtration studies observed significant differences in parvovirus retention depending on particular filtration conditions. However, these observations are poorly understood due to the limited information obtained from the conventional viral load reduction measurements. To better explain these differences, it is essential to visualize the retained parvoviruses in the membrane using a technique that is compatible with a wide range of operating conditions. The objective of this work was to establish and validate a method to accurately detect the retention profile of fluorescently labeled parvoviruses MVM and CPV in filter membranes using LSM and thus to provide the first insights into the filtration of these worst-case parvoviruses.

2. Materials and methods

2.1. Cells and viruses

Minute virus of mice prototype strain (MVMp) was obtained from ATCC and CPV strain Witte originated from Hoechst Roussel Vet GmbH. A plasmid encoding the bacteriophage MS2 coat protein for the expression of recombinant MS2 virus-like particles (VLPs) was purchased from GenScript (Nanjing, China). Mouse A9 fibroblasts were obtained from ATCC and cultured in Dulbecco's modified Eagle's medium (DMEM), 5% fetal calf serum (FCS). Crandel feline kidney (CrFK) cells were kindly provided by T. Nowak (CSL Marburg, Germany) and cultured in Eagle's minimal essential medium (EMEM), 10% FCS. Both mammalian cell cultures were grown at 37 °C, 5% CO_2. Competent BL21 (DE3) *E. coli* cells were obtained from Qiagen (Germany) and cultured in lysogeny broth medium.

2.2. Purification of parvoviruses MVM and CPV

Preparation of highly pure parvoviruses was adapted from a previously published method [32,33]. Semi-confluent mouse A9 fibroblasts and CrFK cells were infected with a high multiplicity of infection of

MVM and CPV, respectively, and harvested 3 days post-infection (dpi) before extensive cell lysis occurred. Cells were washed five times with phosphate-buffered saline (PBS) to remove remaining serum-containing medium and then lysed by three freeze and thaw cycles in 5 mL PBS per T-150 cell culture flask. In contrast to previous approaches, only buffers at neutral pH and without ethylenediaminetetraacetic acid (EDTA) were applied to avoid premature uncoating of viruses [34]. Cell lysate was cleared by low-speed centrifugation at 3000×*g* for 10 min at 4 °C, and incubated with 0.1% Nonidet-P40 (NP-40) for 1 h at 4 °C. The suspension was passed through 0.45 μm and 0.22 μm filters, layered on a 20% sucrose cushion in PBS, 1 mM $MgCl_2$, 0.1% NP-40 provided in an OptiSeal Tube (Beckman Coulter, USA) and ultracentrifuged at 150000×*g* for 3 h at 4 °C in a Ti70 rotor (Beckman Coulter). The pellet was resuspended in 1 mL bottom fraction, diluted with PBS (1:1) and ultracentrifuged again on a 20% sucrose cushion in PBS, 1 mM $MgCl_2$ at 150000×*g* for 3 h at 4 °C in a TLA 100.3 rotor (Beckman Coulter). Fractions were collected from the top for virus quantification and purity analysis.

2.3. Expression and purification of recombinant MS2 VLPs

Expression and purification of MS2 VLPs was performed as previously described [35]. A plasmid vector with MS2 coat protein insert downstream of a T7 promoter was transformed into BL21(DE3) cells and selected with ampicillin. Overnight starter culture was diluted and grown to an optical density (OD_{600}) of 0.4 to induce MS2 coat protein expression with 1 mM isopropyl-β-D-thiogalactopyranoside (IPTG) for 16 h. Cell pellets were collected, resuspended in PBS and lysed by three freeze and thaw cycles and sonication on ice (15 × 10 s). The lysate was cleared by centrifugation at 10000×*g* for 30 min at 4 °C. The supernatant was treated with 0.1% NP-40 and ultracentrifuged on a 20% sucrose cushion, PBS, 0.1% NP-40 at 150000×*g* for 3 h at 4 °C. MS2 VLPs in the pellet were resuspended in the bottom fraction, diluted in PBS (1:3) and layered on a continuous iodixanol gradient (5–60% in PBS) for ultracentrifugation at 150000×*g* for 20 h at 4 °C in a SW-41 rotor. Fractions were collected for VLP quantification and purity analysis.

2.4. Parvovirus quantification by qPCR

Concentration of parvovirus virions was determined by quantitative polymerase chain reaction (qPCR) using the Luna qPCR mix (New England Biolabs, USA) and virus-specific primers as previously described [36]. MVM: forward (5′-GACGCACAGAAAGAGAGTAACCAA-3′ from nucleotides 231 to 254) and reverse (5′-CCAACCATCTGCTCCAGTAAACAT-3′ from nucleotides 709 to 732), resulting in a 501 base pair amplicon. CPV: forward (5′-GACTTAGAGACACAAGCGGCAAG-3′ from nucleotides 1741 to 1763) and reverse (5′-TGCCATCGTACCTTAATCCAAGTCG-3′ from nucleotides 1995 to 2019), resulting in a 278 base pair amplicon. External standards for the respective viruses were generated using the infectious clone of MVM [37] or by cloning an insert of the CPV NS1 gene (nucleotides 1695 to 2048) into a plasmid vector. Amplification and real-time detection of the PCR reaction was performed using the CFX96 Real-Time system (Bio-Rad, USA).

2.5. Quantification of viral capsids

qPCR or infectivity assays are not optimal for an exact particle quantification as the preparation of parvoviruses from cell culture usually contains a major proportion of empty capsids [38,39]. To evaluate the total number of viral capsids, virus proteins were quantified by absorption at 280 nm (A_{280}) using NanoDrop (Qiagen, Germany) and densitometric analysis of Coomassie-stained sodium dodecyl sulfate polyacrylamide gel electrophoresis (SDS-PAGE) referring to a known bovine serum albumin (BSA) concentration for calibration.

2.6. Integrity testing of viral capsids

Bacteriophage MS2 VLPs were analyzed by agarose gel electrophoresis (AGE) and SYBR Gold staining (Thermo Fisher, USA) as previously described [35,40]. The capsid stability and integrity of parvoviruses was tested by a fluorometric assay [41], measuring the temperature-dependent SYBR Gold intercalation into the viral genome. Parvovirus capsids are very compact and hence exclude intercalating dyes in their native conformation, but a signal increase is observed when the genome is exposed under denaturing conditions. SYBR Gold (0.5 × concentration) was added to 5 × 10^9 MVM virions at 4 °C in 20 μl PBS and fluorescence (λ_{ex} 495 nm; λ_{em} 520 nm) was detected with the CFX96 Real-Time system as function of the temperature increase (2 °C/min). To consider changes in fluorescence due to the temperature-dependent melting of the DNA and the background signal of unbound SYBR Gold, the signal was normalized to the temperature-dependent baseline signal of denatured virions as previously described [41].

2.7. Labeling of viruses with amine-reactive Atto dyes

Purified virus suspensions were adjusted to 0.2–1 mg/mL virus protein in PBS, pH 7.4 and incubated with 50 μM of amine-reactive N-hydroxy-succinimide ester-modified Atto dyes (NHS-Atto; Atto-Tec, Germany) for 1 h at room temperature and overnight at 4 °C. The reaction was quenched by adding 50 mM Tris-HCl, pH 8, for 15 min at room temperature. Labeled virions were separated from non-reacted dyes by an additional ultracentrifugation on a 20% sucrose cushion in PBS, 1 mM $MgCl_2$ as describe above. The degree of labeling (DOL) was determined according to the manufacturer's instructions and as previously described [22,42], analyzing the absorption of the labeled viruses at A_{280} with the extinction coefficient of the viral proteins and maximal absorption (A_{max}) of the corresponding fluorescent dye. DOL per capsid was calculated with respect to the number of proteins per capsid (MVM: 60; MS2 VLPs: 180). UV-VIS spectrum of conjugated fluorophore in comparison to free dye only showed a minor proportion of blue-shifted absorption due to self-quenching of aggregated dye (maximal 22%) even at high DOL per capsid [43]. Virus-specific labeling and accuracy of spectroscopic DOL measurement was further confirmed by Coomassie-stained SDS-PAGE and mass spectrometry of Atto-633 modified MS2 VLPs. Mass spectrometry of ZipTip C_{18} purified MS2-633 was performed by matrix-assisted laser desorption/ionization-time-of-flight (MALDI-TOF) in the positive ion mode using alpha-cyano-4-hydroxycinnamic acid (CHCA) as matrix.

2.8. Dynamic light scattering of purified viruses

To determine the hydrodynamic radius of viral particles by dynamic light scattering (DLS), the virus suspensions were additionally purified by ultrafiltration using Amicon filters with a 100 kDa cutoff (Merck Millipore, USA). Samples were diluted 1:10 in PBS and concentrated three times to remove remaining additives that could potentially interfere with the DLS measurement. Purified samples were analyzed at 25 °C using the Zetasizer Nano S instrument (Malvern Instruments, UK). The mean hydrodynamic diameter of the viral particles was calculated on the intensity-based size distribution (Supplementary Fig. 1A and B).

2.9. Anion exchange chromatography

Anion exchange chromatography (AEX) experiments were carried out on a ÄKTApurifier 10/100 UPC-900 chromatography system supported by the Unicorn software (GE Healthcare Life Sciences, USA), and using a Mono Q HR 5/5 AEX column (5 × 50 mm). Purified virus suspensions were spiked into 80 mM BisTris buffer, 40 mM NaCl, pH 7, and injected into a 4 mL loop. The AEX was conducted at a flow of 2.5 mL/min at 10 °C, and 200 μL fractions were collected in 96-well plates (Supplementary Fig. 2). Elution of the viral particles was induced with

an increasing salt gradient up to 2 M NaCl in 80 mM BisTris, pH 7. Elution of proteins was measured during the AEX by absorption (A_{280}). Fluorescence in the fractions was detected with the Microplate Reader Infinite M1000 Pro (Tecan, Switzerland).

2.10. Nanofiltration of Atto-labeled viruses

All filtrations were performed in dead-end mode using commercially available 47 mm Pegasus SV4 filter membranes (Pall Corporation, USA) of the same filter lot and following the manufacturer's instructions. Wetted filter membranes were fixed in a polycarbonate filter holder with a filtration area of 12.5 cm^2 (Sartorius, Germany) downstream of a pressurized feed vessel. All filtrations were carried out at room temperature (21–25 °C) and constant pressure of 2.1 bar. Each filter was checked for filter flow and integrity before use. For virus filtration experiments, 10 mL PBS were spiked with 1 μg of different virus capsids, corresponding to 1.5×10^{11} parvoviruses or 2.4×10^{11} MS2 VLPs. In order to remove potential aggregates in the feed, virus-spiked PBS was filtered through a 0.1 μm PVDF filter (Merck Millipore, USA) prior to nanofiltration. Analysis by qPCR and dot blot did not show any significant decrease of MVM, CPV or MS2 VLPs by the 0.1 μm pre-filtration (Supplementary Fig. 4A). Filtration was performed until the feed volume passed and flow stopped. Virus filter membranes were dried for 1 h at room temperature to dry-fix particles in the membrane.

2.11. Post-filtration staining of retained viruses

To label the retained viruses in the membrane after filtration, the dried membrane was rehydrated with PBS, pH 7.4 and incubated with 50 μM lysine-reactive NHS-Atto-542 for 16 h at room temperature. The membrane was rinsed three times and washed ten times for 30 min with PBS to remove non-reacted dye.

2.12. Determination of the virus retention profile using LSM

Membrane pieces of about 8 × 8 mm were cut out, rehydrated using 10% glycerol in PBS, mounted between a microscope glass slide and coverslip, and sealed with nail polish. Mounted membrane samples were analyzed using the laser scanning microscope 880 with a 63 × magnification objective (Carl Zeiss, Germany). Lasers were run at 2% transmission and detector gain was set using the range indicator to establish an appropriate signal-to-noise ratio. The membrane was scanned with one optical section per micrometer, averaged bi-directional scan, 16-bit depth, and a scan speed of 9. To accurately set the membrane dimensions, the autofluorescence of the PVDF membrane at λ_{ex} 425 nm; λ_{em} 485 nm was measured. Acquired data was processed with the ZEN program for three-dimensional reconstruction, moderate digital enhancement of the signal and virtual cross-sectioning of the scanned filter segment. Cross-sections of multiple acquisitions ($n \geq 3$) were exported as TIFF images and analyzed with ImageJ program [44] and GraphPad Prism to obtain retention profiles with confidence intervals as a function of the filter depth.

2.13. Quantification of parvovirus reduction by qPCR

The viral load was detected in feed and pooled filtrate samples by qPCR with or without nuclease treatment before DNA extraction as previously described [45,46]. Nuclease treatment of virus samples in PBS was conducted with 4000 U/mL micrococcal nuclease (New England Biolabs) in the manufacturer's 1 × nuclease buffer, 1 × BSA and additional 10 mM $CaCl_2$ for 1 h at 37 °C. EDTA (20 mM) was added to stop the nuclease digestion and to resolve calcium phosphate precipitations. Effectiveness of the nuclease digestion was confirmed by spiking representative amounts of infectious clone plasmids into the reaction, showing a reduction of naked DNA by more than 3.6 $\log_{10}$ in the used filtration buffer (Supplementary Fig. 4B). DNA was extracted (DNeasy Blood and Tissue Kit; Qiagen, Germany) and quantified by PCR as described above. The qPCR was designed to be virus-specific, thus allowing the comparison of MVM and CPV in co-spiking filtration experiments (Supplementary Fig. 4C). LRVs of the viral load was calculated according to previous reports [45,46].

2.14. Detection of MS2 VLPs by dot blot after virus filtration

To detect low amounts of MS2 VLPs by dot blot, feed and filtrate samples were concentrated 1000-fold using centrifugal ultrafiltration (100 kDa, Amicon) and spotted on a nitrocellulose membrane. MS2 proteins were detected with an anti-MS2 coat protein antibody (rabbit, Millipore) and horse-radish peroxidase (HRP)-labeled anti-rabbit antibody (goat, Dako). Chemiluminescence detection was performed with SuperSignal Femto Substrate (Thermo Fisher) and Amersham Hyperfilm ECL (GE Healthcare).

To determine the LRV, duplicates of feed samples were spotted as 0.25 $\log_{10}$ dilutions on the nitrocellulose as reference standard. To ensure a comparable ultrafiltration efficiency for MS2 VLPs in feed and filtrate samples, feed samples were pre-diluted by 3.5 $\log_{10}$ to obtain a similar MS2 protein starting quantity as in filtrate samples. LRVs were calculated based on densitometric determination of MS2-positive dots and calibration using the ImageJ program [44]. Detection limit of the dot blot method was an LRV of 4.5 $\log_{10}$.

3. Results and discussion

Direct insight into parvovirus nanofiltration is needed to better understand critical factors that influence the virus retention during a worst-case scenario in the manufacturing of biotherapeutics. The aim of this study was to establish and validate a method to visualize fluorescently labeled parvoviruses inside the virus filters by using LSM to characterize their retention profile.

3.1. Purification and concentration of parvoviruses

While bacteriophages can easily reach high titers by expression in prokaryotic cells, mammalian viruses as parvoviruses generally show a significantly lower yield in the corresponding cell culture systems. Therefore, a major challenge of this study was to obtain sufficient amounts of parvoviruses with a high purity for an efficient and specific labeling. According to previous protocols [32,33], we collected intracellular parvoviruses MVM and CPV 3 dpi when cytopathic effects were visible but before extensive lysis of the cells occurs. To concentrate and purify viral capsids, we employed two ultracentrifugation steps through 20% sucrose cushions, enriching the viruses based on their higher capsid buoyant density compared to cellular impurities. The virus concentration in the ultracentrifugation fractions was determined with qPCR, showing a final enrichment of parvoviruses in the second pellet fraction of 100-fold (Fig. 1A and B). SDS-PAGE and Coomassie stain analysis indicated that parvoviruses were specifically concentrated with this method while cellular contaminants were effectively removed to almost undetectable levels (Fig. 1C).

The purity of the virus is an essential requirement to ensure a reproducible virus-specific labeling and to eliminate artifacts in the detection, as the amine-reactive fluorescent dye would crosslink to viral capsids as well as to protein impurities. Furthermore, working with pure virus stocks allows an accurate quantification of the viral particles for appropriate virus spiking in the filtration experiments [47], and minimizes unwanted fouling effects caused by remaining cellular impurities such as host cell proteins and DNA [26,33,48–50].

3.2. Preparation of pure bacteriophage MS2 VLPs

Small bacteriophages are frequently employed as parvovirus surrogates due to their low cost and ease of production [51]. To evaluate

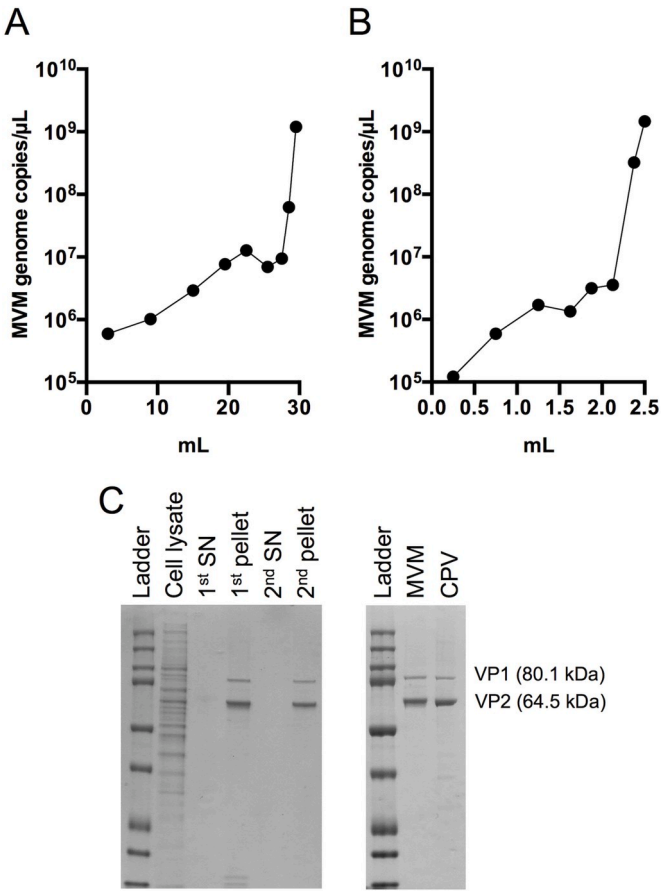

Fig. 1. Purification of parvoviruses MVM and CPV. A) Purification of MVM from A9 cell lysate three days post-infection by sucrose cushion (20%) ultracentrifugation and detection of viral genomes in sampled fractions by qPCR. Fractions were taken from the top towards the bottom of the tube (0–30 mL). B) MVM detected in fractions from a second sucrose cushion ultracentrifugation in 2.5 mL (qPCR). C) Coomassie-stained SDS-PAGE of supernatant and pellet fractions of both sucrose ultracentrifugations and (D) final parvovirus stocks of MVM and CPV.

whether bacteriophages accurately reflect the retention of relevant parvoviruses in filter membranes, it was of interest to include one of these surrogates in our study. To this end, we prepared VLPs of bacteriophage MS2 by recombinant expression of the MS2 coat protein (13.6 kDa) in *E. coli*. MS2 VLPs share most physicochemical properties with native MS2 bacteriophages, as the particles consist of the same coat protein and only lacks the encapsidated viral ssRNA genome and the maturase protein. The VLPs encapsidate some cellular RNA during expression, rendering the particles detectable for intercalating dyes such as SYBR Gold. The recombinant production of VLPs represents a convenient alternative to native bacteriophages, as this approach offers an inducible and well-controlled overexpression of particles. To obtain highly pure viral particles, MS2 capsids were purified by one sucrose cushion ultracentrifugation (Fig. 2A) and one iodixanol density gradient ultracentrifugation (Fig. 2B).

3.3. Identity and integrity of viruses

To verify the identity of parvoviruses and MS2 VLPs, we used virus-specific qPCR (Fig. 1A and B), Western Blot and AGE (Fig. 2C and D). Furthermore, we controlled the integrity of the viral particles prior to labeling as defective viruses may show an altered retention in the filtration experiments. The sucrose cushion ultracentrifugation (Fig. 1A and B) and the additional iodixanol density gradient ultracentrifugation (Figs. 2B and 3A) confirmed the integrity of the virus particles as the capsids pelleted and migrated with the typical buoyant density of intact viruses [39]. The staining of heat-denatured iodixanol fractions with SYBR Gold showed only significant signal in the MVM containing fractions, demonstrating that the viral preparation did not contain nucleic acid contaminants besides the encapsidated viral genomes (Fig. 3A).

The integrity and stability of the parvovirus particles was additionally corroborated by exclusion of SYBR Gold from the native parvovirus capsids and temperature-dependent signal increase due to genome exposure, as previously reported with Dependoparvoviruses (Fig. 3B) [41]. In contrast, SYBR Gold entered the MS2 VLPs through the larger pores present in the capsid of this virus [52] in a temperature-independent manner. The exclusion of intercalating dyes from MVM virions demonstrates that pre-labeling with SYBR Gold is not applicable for parvoviruses, as it has previously been employed for bacteriophages [23] and further emphasized the important structural differences between bacteriophages and parvoviruses. In the native AGE, MS2 VLPs migrated at the expected distance and were resistant to Benzonase (Fig. 2D), confirming an intact capsid structure [35,40].

3.4. Labeling of viruses with fluorescent dyes

The objective of the fluorescent labeling was to achieve sufficient modifications for a convenient detection of the virus, but without significantly changing the physicochemical properties of the capsids, which would affect the viral retention in the filter membrane. Purified viral particles were labeled with different amine-reactive NHS-Atto dyes (Table 1) in PBS at pH 7.4.

Non-reacted fluorophores were separated from labeled viruses by an additional sucrose cushion ultracentrifugation step. Since modifications of the capsid surface can potentially alter the charge and size of the

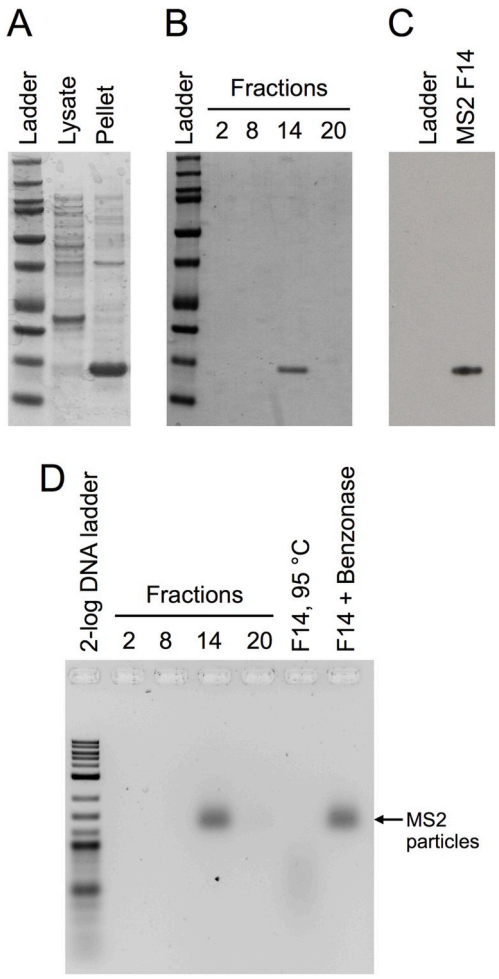

Fig. 2. Expression and purification of bacteriophage MS2 virus-like particles (VLPs). A) SDS-PAGE of recombinantly expressed MS2 VLPs purified from *E. coli* cell lysate by sucrose cushion ultracentrifugation and (B) iodixanol gradient (5–60%) ultracentrifugation. Fractions 2, 8, 14 and 20 were selected to represent the entire iodixanol gradient (22 fractions total). Peak of protein content was detected in fraction 14. C) Western blot of the iodixanol gradient fraction 14 using an anti-MS2 antibody and HRP-labeled secondary antibody. D) Agarose gel electrophoresis (1.2%) of selected iodixanol fractions stained with SYBR Gold. Lane 6 and 7 show samples of fraction 14 treated with heat (95 °C, 5 min) or Benzonase (1 U), respectively.

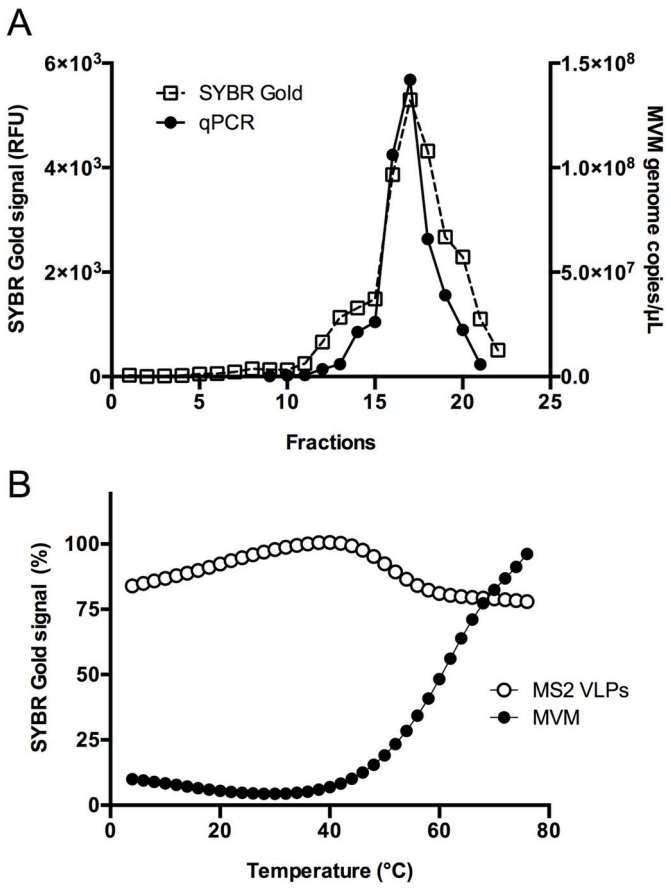

Fig. 3. Fluorometric SYBR Gold assay of purified MVM and MS2 VLPs. A) Iodixanol gradient ultracentrifugation (5–60%) of purified MVM and detection of MVM genomes by qPCR and by SYBR Gold after denaturation of samples by heat treatment (95 °C). B) Fluorometric assay based on SYBR Gold intercalation to test the integrity and stability of parvovirus capsids. Detected signal of SYBR Gold in purified MVM virions (fraction 17) and MS2 VLPs (fraction 14), shown by the relative fluorescence (RFU) as a function of temperature increase (2 °C/1 min). Relative fluorescence was normalized to baseline signal of a denatured virus samples.

virus, the DOL per capsid is a critical parameter to be controlled to obtain reproducible results. The DOL per capsid was quantified by spectrometric analysis as previously described based on the absorption of proteins and fluorescent dyes (Table 2) [22,42].

Labeling of MVM with 50 µM NHS-Atto-633 resulted in 16.8 fluorophores per virus (MVM-633), which corresponds to 0.21% of the capsids mass. Comparable labeling efficiencies of MVM and MS2 VLPs were achieved with NHS-Atto-542 and NHS-Atto-488 fluorophores (DOL 14.7–21.7) using the same dye concentration (Table 2). An about three times lower labeling (MVM-$633_{1/3}$; DOL per capsid = 4.9) was obtained with 10 µM fluorophore in the labeling reaction. Interestingly, labeling of MS2 VLPs with 50 µM of NHS-Atto-633 resulted in 37.2 modifications per capsid. The high DOL per MS2 particle with Atto-633 can be explained by the large pores present in the bacteriophage capsid, allowing this particularly small and positively charged dye to enter similar to SYBR Gold (Fig. 3) and crosslink also with lysines in the interior of the particle. However, an influence of the additional Atto-633 labeling on the physicochemical properties of the MS2 VLPs can be excluded as an internal modification does not modify the size or surface characteristics of the virus.

Furthermore, the virus-specific labeling and DOL were controlled by SDS-PAGE and mass spectrometry (Fig. 4).

The SDS PAGE of Atto-633 labeled MVM indicates virtually the same migration of MVM-$633_{1/3}$ proteins compared to non-modified MVM proteins (Fig. 4A). In contrast, MVM-633 proteins show a detectable but only minor mass shift in the SDS PAGE. Taken together, the visual analysis confirms the virus-specific labeling with a limited number of dyes per MVM capsid. Since the MS2 coat protein (13.6 kDa) has a smaller mass compared to MVM viral proteins (62–80.1 kDa), the Atto-633 modification of an MS2 coat protein can be detected by a significant

Table 1
Overview of amine-reactive N-hydroxysuccinimide modified Atto-fluorophores (NHS-Atto) used to label capsids for virus filtrations. Δm: increase of molecular mass on conjugation with dye; Δq: increase of electrical charge on conjugation with dye [53].

Fluorophores	Δm (Da)	Solubility	Δq	Stability
NHS-Atto-425	383.4	moderately hydrophilic	0	stable
NHS-Atto-488	570.6	very hydrophilic	−1	stable
NHS-Atto-520	349.5	hydrophobic	+1	colorless pH > 7
NHS-Atto-542	893.0	very hydrophilic	−3	stable
NHS-Atto-610	373.5	moderately hydrophilic	+1	stable at pH 2 - 8
NHS-Atto-633	534.7	moderately hydrophilic	+1	stable

Table 2
Characterization of the labeled viruses used for nanofiltration. The degree of labeling (DOL) was determined by the spectrometric absorption of the proteins and dyes. ΔMW (%) indicates the calculated increase of the capsid mass based on the DOL, shown as percentage of total capsid mass (MVM, 4.2 MDa; MS2 VLPs, 2.5 MDa). The hydrodynamic diameter of the viral particles was determined by dynamic light scattering (DLS) based on at least four measurements ($n \geq 4$). Δq indicates the total change of charges on the capsid calculated based on the DOL. The elution profile of a virus in the anion exchange chromatography (AEX) is determined by the capsid surface electrostatics and is represented by the conductivity (mS/cm) measured in the elution peak of the virus.

	Degree of labeling (DOL)	ΔMW (%)	Hydrodynamic diameter (nm)[a]	Δq of capsid	AEX elution (mS/cm)
MVM	0	0	34.4 (±2.6)	0	24.67
MVM-488	14.7	0.20	35.4 (±1.4)	−14.7	23.52
MVM-542	15.9	0.34	36.8 (±2.0)	−47.7	24.81
MVM-633	16.8	0.21	n.a.[d]	+16.8	23.52
MVM-$633_{1/3}$	4.9	0.06	n.a.[d]	+4.9	–
MS2 VLPs	0	0	31.9 (±1.6)	0	34.33
MS2-488	21.7	0.50	34.7 (±1.8)	−21.7	33.69
MS2-542	15.3	0.55	30.7 (±1.0)	−45.9	33.69
MS2-633	37.2/44.5[b]/45.5[c]	0.80	n.a.[d]	+37.2	31.91

[a] according to the intensity-based size distribution.
[b] determined by MALDI-TOF MS.
[c] determined by SDS PAGE.
[d] absorption of the Atto-633 dye interferes with DLS analysis and hence is not applicable (n.a.).

mass shift on the SDS-PAGE (Fig. 4B) as well as with MALDI-TOF mass spectrometry (Fig. 4C). Quantification of the shifted population showed a similar DOL determined by the different analytical methods used: SDS-PAGE (DOL = 45.5), MALDI-TOF (DOL = 44.5) and UV-VIS absorption (DOL = 37.2).

To evaluate whether the type of labeling may influence the retention of the virus, we labeled the viruses with six different dyes, each with characteristic properties regarding mass, hydrophobicity and charge (Table 1).

3.5. Size and capsid surface electrostatics of labeled viruses

To determine whether the modification of the viruses with a limited number of fluorophores significantly changed the size or surface electrostatics of the capsids, we analyzed the labeled viruses by dynamic light scattering (DLS) and anion exchange chromatography (AEX), respectively. The DLS measurement of the virus suspensions showed a single peak in the volume-based size distribution, confirming a monodisperse and pure virus preparation (Supplementary Fig. 1B and D). The comparison of non-labeled with labeled viruses revealed no significant increase of the hydrodynamic diameter of the capsids, which reflects the apparent size of the hydrated viral particles in solution (Table 2,

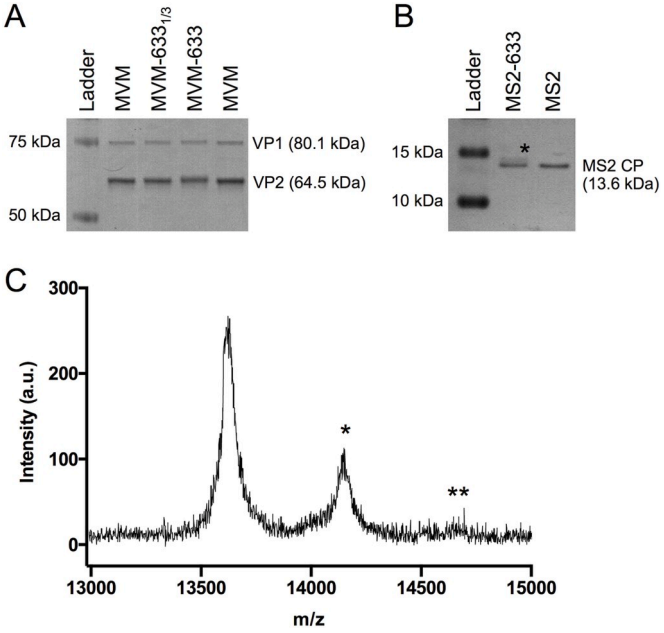

Fig. 4. Determination of the degree of labeling (DOL) per capsid. A) Coomassie-stained SDS-PAGE of purified MVM labeled with different amounts of Atto-633 fluorophores. MVM: unlabeled virus; MVM-$633_{1/3}$: 4.9 Atto-633 dyes per capsid; MVM-633: 16.8 Atto-633 dyes per capsid. B) SDS-PAGE of Atto-633 modified MS2-VLPs. C) Mass spectrometry of MS2 VLPs modified with NHS-Atto-633 dye, showing a minor proportion of Atto-633 labeled MS2 coat proteins (24.7%) in comparison with unlabeled protein (75.3%). Asterisks show MS2 coat protein (MS2 CP) modified with one (*) or two (**) Atto-633 dyes.

Supplementary Fig. 1A and C), even with the largest dyes attached. This observation was not unexpected, as the low DOL per virus represents only 0.06–0.80% of the capsid mass (Table 2) and such marginal differences likely remain undetectable in the DLS measurements. Furthermore, it should be considered that the DLS estimates the mean hydrodynamic diameter assuming the particles as perfect spheres, while fluorophore modifications only add very small protrusions on the already uneven surface of viral particles. Although undetectable in the DLS, these few additional residues may still increase the maximal diameter of the capsid in certain orientations and hence potentially influence the movement of the particle in the porous network of a virus filter membrane.

To test whether the few modifications on the capsid surface change the electrostatics of the virus and thus the charge-dependent adsorption to surfaces as it may occur during nanofiltration, we performed an AEX at neutral pH and eluted the virus by an increasing salt gradient. No significant differences in the adsorption and elution were observed between labeled and unlabeled viruses (Table 2, Supplementary Fig. 2). Taken together, the very limited number of fluorophores per capsid did not cause any significant change in the hydrodynamic diameter or surface electrostatics of the viruses.

3.6. Filtration of labeled viruses

Virus filtration experiments were all performed using Pegasus SV4 double layer membrane filters with a nominal pore size of 20 nm. These membranes have a symmetrical porous structure and consists of hydrophilic acrylate-modified PVDF polymer [14]. Operation conditions were applied following the manufacturer's instructions, keeping a constant pressure of 2.1 bar. According to PDA standardization, all virus filtrations were performed in PBS, pH 7.4 [54]. Virus spike containing 1 μg viral proteins were applied into the feedstream, corresponding to a total viral load of 1.5–2.4 $\times$ 10^{11} particles per 0.001 m^2. Filter flow decay was not detected during the filtration time, corresponding with the results of previous studies when highly purified viruses were used [26].

3.7. Detection of fluorophore-labeled MVM using LSM

LSM is a convenient and well-established detection method to acquire optical stacks and to reconstruct three-dimensional images from fluorescent signals. A critical parameter, however, is the exact localization of the fluorescent signal in relation to the membrane depth to reproducibly compare acquisitions from different experiments. For this purpose, the autofluorescence of the PVDF filter membrane was measured at λ_{ex} 425 nm; λ_{em} 485 nm to accurately set the boundaries for the filter dimensions (Fig. 5A). Notably, the first 2–4 μm of the membrane showed a detectable, but rather low autofluorescence compared to the rest of the filter. This lower autofluorescence is likely attributed to a less dense layer at the feed side of membrane.

The Atto-542 and Atto-633-labeled MVM particles (MVM-542 and MVM-633) were filtered in a co-spike experiment and detected by LSM. Both virus labelings resulted in a homogenous and similar retention pattern in the first micrometers of the filter membrane (Fig. 5B and C). However, the comparison of the two fluorescence signals in the merge mode, revealed a deeper migration of MVM-633 compared to MVM-542 (Fig. 5D).

3.8. Determination of MVM retention profiles in the filter membrane using different labeling dyes

A profile of the fluorescent signal as a function of the filter depth was generated by ImageJ analysis of the acquired data [44]. Based on multiple acquisitions, a confidence interval was established showing the standard deviations at each filter depth. The graphical depiction shows that the retention profile of MVM-542 and MVM-633 are similar regarding the peak of retention, but having an additional accumulation of MVM-633 in a deeper layer of the membrane (Fig. 5E). A secondary effect due to the detection of different wavelengths was excluded, as scanning of the membrane from the opposite direction resulted in the same profile (Supplementary Fig. 3A and B).

Labeling and filtration of MVM with Atto-488 showed a similar pattern as the profile obtained with MVM-542 (Fig. 5F). In contrast, filtration of MVM-520 resulted in a strong accumulation of the signal at the very beginning of the filter and indicated larger variabilities throughout the entire retention profile (Fig. 5F). As this dye has a reported high hydrophobicity (Table 1), the modification with this fluorophore may have caused aggregation of the virus or adsorption to the filter membrane as observed with hydrophobic gold nanoparticles when no anionic detergent was present [20]. Due to this deviating effect, MVM-520 was not used for further experiments. Similarly, labeled MVM-425 and MVM-620 particles could not be used for detection due to high autofluorescence of the PVDF membrane at shorter wavelengths (Fig. 5A) and insufficient stability of the fluorescent dye, respectively (Table 1).

To quantitatively compare the different retention profiles, we defined two critical values that reflect the observed differences: 1) The filter depth of the peak signal, representing the majority of the retained viruses, and 2) the maximal filter depth where 10% of the peak signal is still detected, reflecting the ability of the virus to penetrate into the membrane. No significant differences in the peak depth were found for MVM labeled with the different fluorophores Atto-488, Atto-542 and Atto-633 (Fig. 5G). However, MVM modified with Atto-633 showed an increased maximal filter depth compared to Atto-488 and Atto-542. This comparison revealed that the type of labeling itself has an influence on the retention in the filter, a factor that has not been considered in the previous studies, but which is crucial to accurately compare different viruses.

3.9. Influence of the labeling on the retention of different viruses

To assess whether the influence of the used fluorescent dyes is specific for MVM only or similar for different viruses, we labeled CPV and MS2 VLPs with the same type of dyes (Tables 1 and 2). The retention profiles of CPV-542 and CPV-633 were very similar to those of MVM (Fig. 6A). While the peaks of both labelings were found in the same filter depth, CPV modified with Atto-633 showed again a migration to deeper layers compared to CPV-542 (Fig. 6C).

Interestingly, a deeper retention profile was observed with fluorophore-labeled MS2 VLPs (Fig. 6B), suggesting that the recombinant MS2 particles have a smaller apparent size compared to parvovirus capsids. The deeper migration of the MS2 VLPs cannot be simply attributed to the lacking genome, since a large proportion of the labeled parvoviruses are also empty, but do not show this significantly deeper retention. The fluorescent dyes exhibited a similar but even stronger influence on MS2 VLPs, affecting not only the maximal retention depth but also the depth of the peak (Fig. 6D). This observation would imply that capsid modifications increasingly influence the migration as the virus diameter gets closer to the nominal pore size of the filter membrane.

Taken together, these results show that the labeling with a particular dye has a very similar impact on the different viruses. Each type of fluorescent dye exhibited a characteristic effect on the migration of the viruses in the membrane with decreasing retention from Atto-542 > Atto-488 > Atto-633. Considering that size exclusion plays a predominant role at normal flow conditions and that the influence on the viral retention was in the order of the molecular weight of the dyes (Table 1), it is tempting to speculate that the difference in the retention was primarily caused by the very small additional protrusions on the virus surface. A significant influence of the adsorption-related properties, i.e. charge or hydrophobicity, appears rather unlikely, since the labeled and unlabeled viruses indicated a very similar interaction and elution profile

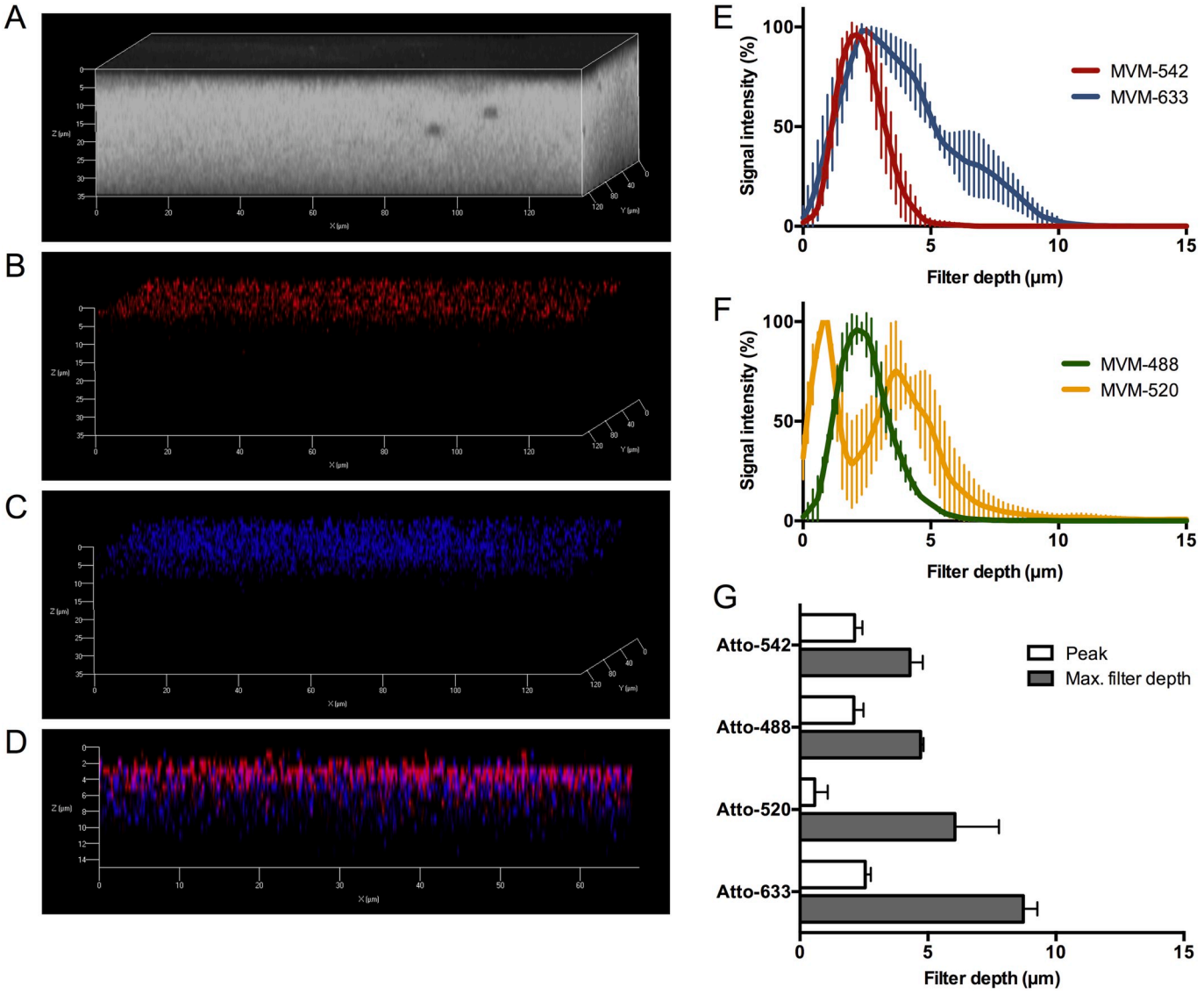

Fig. 5. Laser scanning microscopy (LSM) of Pegasus SV4 membrane after filtration of PBS feedstream spiked with fluorophore-labeled MVM. A) Detection of filter membrane dimensions based on the autofluorescence of the PVDF membrane at λ_{abs} 425 nm and λ_{em} 485 nm to set the laser scanning lattice for virus detection. Three-dimensional reconstruction of retained MVM modified with (B) Atto-542 or (C) Atto-633. D) Virtual cross-sections of the virus filter membrane showing the retained MVM-542 and MVM-633. E) Retention profile of MVM-542 and MVM-633 determined by ImageJ analysis of the fluorescent signal as a function the filter depth. Peak signal and standard deviations were calculated based on acquisitions of three different membrane areas (n = 3). F) Retention profile of MVM-488 and MVM-520. G) Peak signal and maximal filter depth of retained MVM modified with different fluorescent dyes to compare the influence of the different modifications (n = 3). Maximal filter depth was defined as the value (µm) where the detected signal of the retained viruses decreased to 10% of the peak signal.

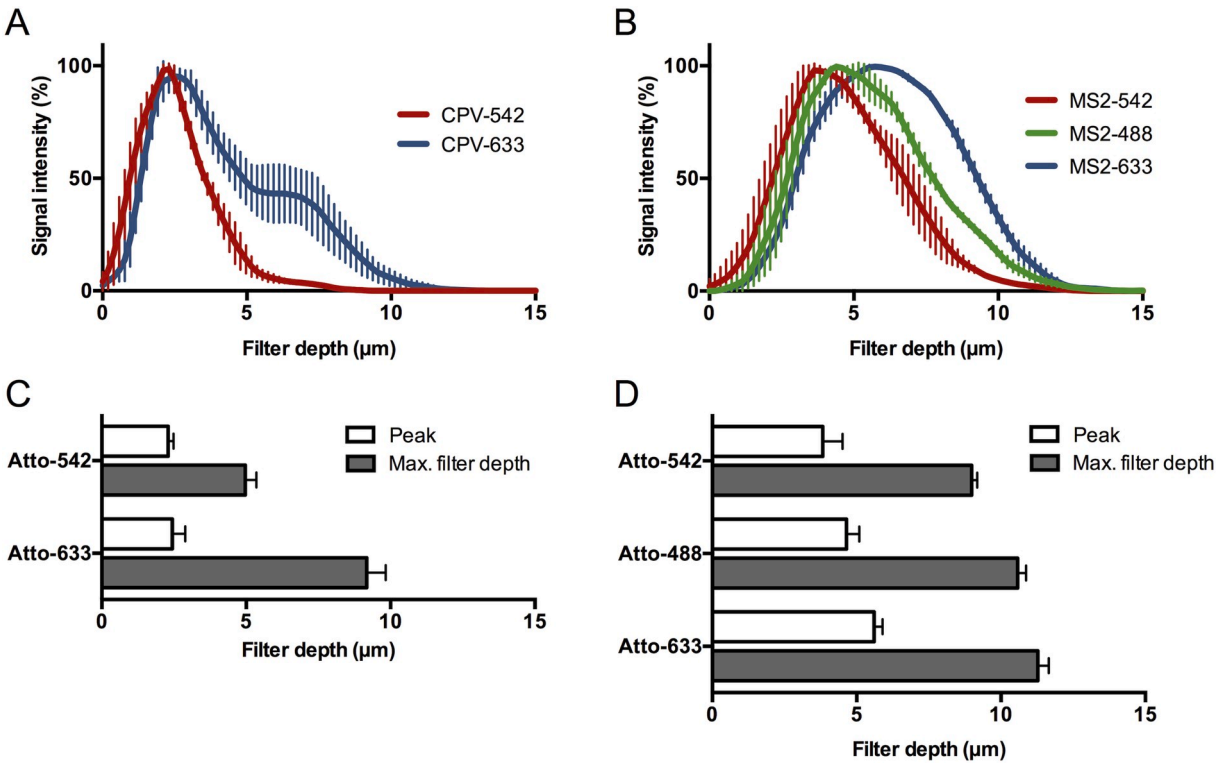

Fig. 6. Influence of different fluorophore modifications on the retention of CPV and MS2 VLPs in the filter membrane. Retention profiles of (A) CPV and (B) MS2 VLPs modified with the different fluorophores Atto-542, Atto-633 or Atto-488 shown as a function of the filter depth. Confidence interval based on standard deviations from three independent acquisitions (n = 3). Peak signal and maximal filter depth of modified (C) CPV and (D) MS2 VLPs (n = 3).

in the AEX (Table 2, Supplementary Fig. 2). Nevertheless, an impact of the surface characteristics of the capsids on the retention should not be totally excluded, especially if the virus filtration is performed under low operating pressure [29].

3.10. Minimizing the effect of the labeling on virus retention

To estimate the remaining influence of the lowest-affecting Atto-633 dye on MVM retention, we additionally prepared MVM with about three times less labelings per capsid (MVM-$633_{1/3}$; DOL = 4.9) compared to the MVM-633 used above (DOL = 16.9). The retention profile of MVM-$633_{1/3}$ indicated a modest but not significant increase of the signal in deeper layers of the filter membrane compared to the normal labeled MVM-633 (Fig. 7). The limited effect on the retention profile with a low DOL per capsid suggests that the retention pattern of MVM-633 is close to that of unlabeled MVM.

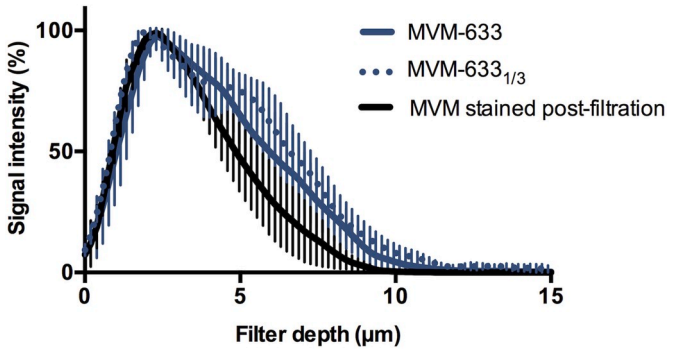

Fig. 7. Comparison of MVM labeled pre-filtration with different numbers of Atto-633 fluorophores or stained post-filtration in the membrane. Blue curves show the retention profiles of pre-filtration labeled MVM-633 (16.8 dyes per capsid) and MVM-$633_{1/3}$ (4.9 dyes per capsid). Unlabeled MVM was filtered and stained post-filtration with the hydrophilic Atto-542 dye for 16 h. Retention profiles as function of the filter depth show mean and standard deviation of acquisitions from three different membrane areas (n = 3). (For interpretation of the references to color in this figure legend, the reader is referred to the Web version of this article.)

To visualize the retention profile of MVM filtered without any modifications, we stained the virus in the membrane post-filtration using the hydrophilic NHS-Atto-542 dye. The post-filtration labeling resulted in the same filter depth of the peak signal as the pre-filtration labeling (Fig. 7). However, in contrast to the MVM-633 pre-filtration labeling, the signal obtained by post-filtration labeling did not detect the viruses detected in deeper layers. This observation implies that post-filtration staining may only efficiently label particles close to the surface of the membrane and thus may underestimate deeper migrating viruses. Therefore, modification of viral particles pre-filtration with a limited number of fluorophores that have a negligible impact on the virus migration like the Atto-633 dye, allows a more accurate detection of the virus retention profile than labeling of retained viruses post-filtration.

3.11. Determination of parvovirus LRVs using qPCR

To evaluate the effect of the labeling on the breakthrough of viral particles, we used virus-specific qPCR (Supplementary Fig. 4C), analyzing the concentration of viral DNA in the feed and filtrate to determine the LRV as previously described (Table 3) [45,46].

The detection of viruses by qPCR was preferred to the frequently used infectivity assays, since we sought to directly detect particles and to exclude a potentially biased infectivity due the modification of the virus by the different fluorophores. In order to ensure that the qPCR measurement only detects viral particles and not possibly decapsidated viral DNA, we treated one set of samples with micrococcal nuclease before DNA extraction. The nuclease treatment of the samples appeared to be a necessary step, as the analysis without nuclease digestion generally

Table 3
Logarithmic reduction values (LRVs) of MVM, CPV and MS2 VLPs. Reduction of the parvovirus load was examined by qPCR. Samples were treated with micrococcal nuclease before DNA extraction to remove non-encapsidated viral DNA. The LRVs based on qPCR detection without nuclease treatment are shown to illustrate the overestimation of viral breakthrough due to the presence of viral DNA fragments in the filtrate. Reduction of MS2 VLPs was measured by dot blot detection of MS2 coat proteins in the feed and filtrate using a specific antibody against the MS2 coat protein and secondary HRP-labeled antibody. Standard deviations were calculated based on at least two independent experiments (n ≥ 2). (*Nuclease treatment is not applicable for dot blot detection of MS2 VLPs.)

Virus	LRV + Nuclease	LRV - Nuclease
CPV	≥6.0 (±0.3)	4.9 (±0.9)
MVM	5.0 (±0.4)	4.2 (±0.3)
CPV-542	6.2 (±0.2)	5.2 (±0.2)
MVM-542	≥5.8 (±0.3)	5.0 (±0.2)
CPV-633	≥6.0 (±0.1)	5.0 (±0.5)
MVM-633	5.6 (±0.4)	5.0 (±0.3)
MVM-$633_{1/3}$	4.9 (±0.3)	4.7 (±0.1)
MS2 VLPs	3.6* (±0.1)	

showed lower LRVs, thus overestimating the breakthrough of viruses. The overestimation of breakthrough was found to be due to decapsidated MVM DNA in the filtrate (data not shown), probably representing genomic fragments that may have been generated during the filtration process as described for B19V [45,46].

The comparison of the LRVs of unlabeled MVM (LRV = 5.0) with the moderately labeled MVM-$633_{1/3}$ (LRV = 4.9) showed that the modification of the capsid with only 4.9 Atto-633 dyes per particle has an undetectable effect on the retention of the virus (Table 3). MVM-633 with 16.9 fluorophores per capsid resulted in a slightly increased LRV (5.6) while showing a virtually identical retention profile in the filter as MVM-$633_{1/3}$ (Fig. 7).

Taken together, the labeling of capsids with a limited number of Atto-633 fluorophores per capsid (DOL of 5–20) represents a suitable method to accurately reflect the retention profile of native unmodified viruses in filter membranes.

3.12. Comparison of different viruses based on the retention profiles and LRVs

Since the modification with a particular type of fluorophore shows a similar effect on the retention of different viruses (Figs. 5 and 6), it is valid to compare the relative migration of viruses in the membrane if they are labeled with the same dye. Therefore, we separately plotted the retention profiles of the parvoviruses MVM, CPV and the bacteriophage MS2 VLPs depending on their modification with Atto-542 (Fig. 8A) or Atto-633 (Fig. 8B). Fig. 8C and D depict the corresponding values for retention peaks and maximal filter depths of the different viruses. The comparison of both modifications consistently shows that the parvoviruses MVM and CPV have a very similar retention pattern, while the recombinant MS2 VLPs migrate significantly deeper into the Pegasus SV4 filter membrane (Fig. 8A and B). In line with this, no significant differences between MVM and CPV are detectable regarding retention peak and maximal filter depth with both modifications (Fig. 8C and D). In contrast, MS2 VLPs show a significantly deeper retention peak and maximal filter depth for the Atto-542 as well as for the Atto-633 modified viruses (Fig. 8A–D).

According to the proposed size-based sieving mechanism of virus filters, smaller particles have the capability to migrate deeper into the complex network of pores and hence have a higher probability to pass through the filter. To evaluate whether the retention profiles in the membrane show a correlation with the virus breakthrough, the viral load reduction of the different model viruses was examined (Table 3). Parvoviruses in the feed and filtrate were detected based on qPCR analysis after nuclease treatment to exclude detection of decapsidated

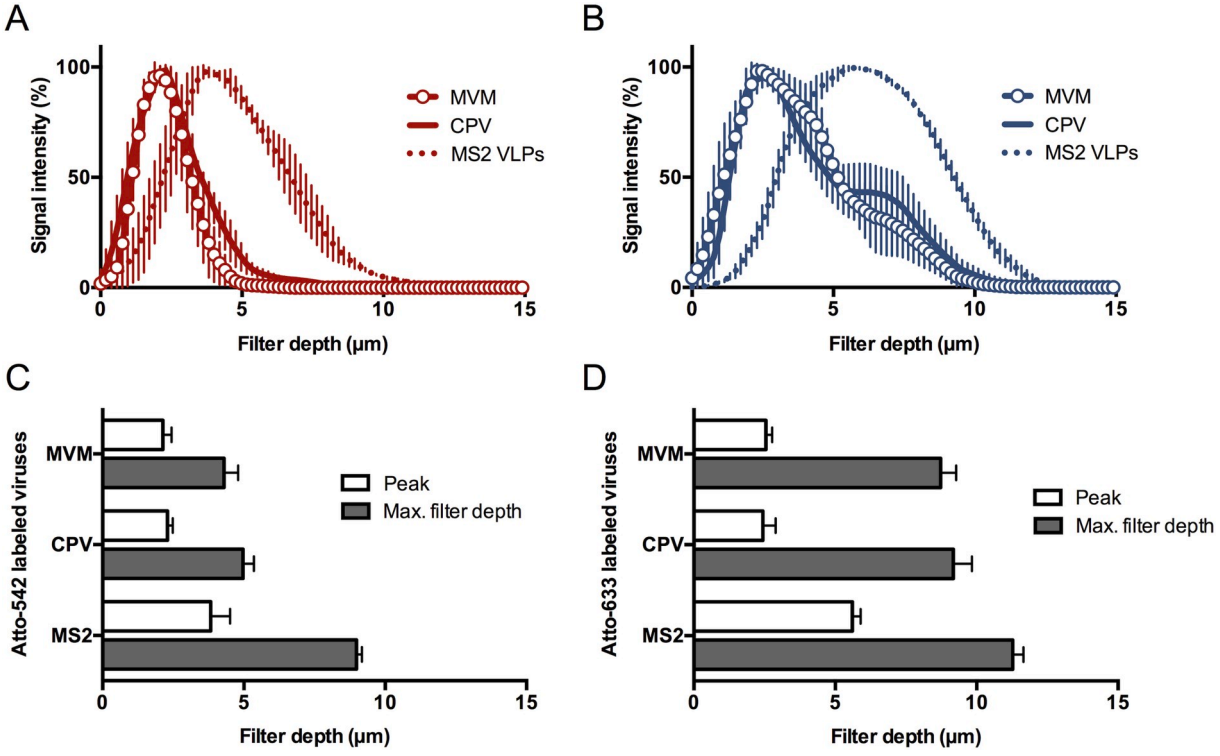

Fig. 8. Comparison of the retention pattern of labeled CPV, MVM and MS2 VLPs in the virus filter membrane as a function of the filter depth. Retention profiles of viruses labeled with (A) Atto-542 and (B) Atto-633, showing a confidence interval of three independent acquisitions (n = 3). Histograms show the depth of the retention peak and maximal filter depth of the different viruses modified with (C) Atto-542 or (D) Atto-633. Standard deviations are calculated based on three independent measurements (n = 3).

DNA fragments. The LRVs of unlabeled or labeled parvoviruses were consistently found at more than 4.9 $\log_{10}$, showing an effective retention of both MVM and CPV under standard filtration conditions in PBS and constant flow, correlating with the observed retention profile in the filter (Fig. 8A and B). In contrast, the previously reported differences between MVM and CPV were observed under product-specific filtration conditions at lower pH and involving significant filter fouling [15]. Generally, the modified virions showed slightly higher LRVs compared to the unlabeled viruses; however, these small differences allow only limited interpretation, as the values are close to the absolute detection limit of the assay (Table 3, Supplementary Fig. 4B).

To measure also the LRV of MS2 VLPs, we established a dot blot analysis of particles in the feed and filtrate using a bacteriophage MS2 coat protein-specific antibody and HRP-based detection. As expected based on the significantly deeper retention of MS2 particles (Fig. 8A–D), the unlabeled MS2 VLPs showed a higher breakthrough of particles (LRV = 3.6) (Supplementary Fig. 5) when compared to the LRVs of unlabeled parvoviruses MVM and CPV (LRV $\geq$ 5.0) (Table 3). This result exemplary shows that a deeper migration into the membrane correlates with a lower LRV, conforming with previous studies where the retention patterns in the filter membrane were linked to virus breakthrough [23,30]. Interestingly, this difference between parvoviruses and MS2 VLPs cannot be explained based on the reported size of the viruses, since their capsids have virtually the same outer capsid diameter (28.4–28.8 nm) [10,11,52]. In accordance with this, the DLS measurement did not reveal a significantly smaller hydrodynamic diameter of MS2 VLPs compared to MVM (Table 2, Supplementary Fig. 1A and B). This finding suggests that minor variabilities in the capsid structure may play a critical role in the retention of the viruses.

The significant differences observed between parvoviruses and MS2 VLPs emphasize that model viruses and particles with a similar size cannot be interchangeably used in virus filtration studies. Replacing the relevant parvoviruses with bacteriophages, VLPs or artificial particles may simplify many aspects of the experiments; however, may also generate results that do not accurately reflect the retention of native parvoviruses. Future studies are warranted to determine to what extent model viruses, VLPs or nanoparticles can represent the behavior of parvoviruses in filtration studies and where the applicability of these models is limited.

The filtration of viruses labeled with different fluorescent dyes revealed that small changes on the viral capsid can have a significant impact on the virus retention in the membrane (Figs. 6 and 7). Considering the small size of the fluorescent molecules, this observation implies that cellular modifications or conformational changes of the capsid can affect the virus removal by nanofiltration. In this context, it is important to note that viruses are not inert particles, but have a build-in capacity to react to their environment. In particular mammalian viruses like parvoviruses need to rearrange during virus entry into the host cell for proper endocytosis, trafficking and uncoating. Viruses from the same family, as parvoviruses, can have fundamental differences regarding conformational changes in response to external triggers [34,55,56]. Hence, it is critical not only to evaluate specific filtration conditions on a case-by-case basis [29], but also to consider that even related parvoviruses may behave very different in certain filtration conditions as recently observed [15]. Taken together, the virus model in filter research studies needs to be carefully chosen to accurately reflect a relevant scenario in the manufacturing of biotherapeutics.

4. Conclusion

Virus filtration is an essential virus clearance step in the manufacturing of biotherapeutics. Although the technique is considered very effective, parvovirus breakthrough has been observed under certain operating conditions. Parvoviruses are considered the worst-case virus challenge for validation studies; however, the mechanism involved in the breakthrough remains poorly characterized due to the limitations of the current experimental approach based on LRV. Accordingly, there is a need to develop novel methods that can allow the direct visualization of the parvovirus particles inside the filter. The primary aim of this study was to apply and validate a method to visualize and characterize the retention profile of model parvoviruses inside the filter membrane by LSM and to identify the most critical factors that influence the process.

To this end, native parvoviruses MVM and CPV were purified from infected cell cultures and labeled with different fluorescent dyes. The identity, capsid integrity and degree of labeling of the viruses was verified prior to filtration to ensure a virus-specific detection in the membrane. Furthermore, by accurate detection and comparison of different scanning acquisitions, we could validate the reproducibility and robustness of the method.

The virus retention profiles revealed minor differences between viruses and capsid modifications with a high resolution, finding that small changes of the capsid surface have a detectable impact on the retention of the virus.

The retention profiles complemented with measurements of the viral load reduction showed that the two parvoviruses MVM and CPV have a very similar retention behavior under standard filtration conditions. In contrast, recombinant MS2 VLPs were found to migrate significantly deeper into the filter membrane. This finding suggests the limited applicability of bacteriophages or nanoparticles as models to study parvovirus retention in the filter membrane. Hence, a potential worst-case scenario in virus filtration can only be accurately visualized by the relevant parvovirus, labeled with a fluorophore that only minimally affects the viral retention.

The detection of the virus retention profile will allow to exactly define the separation-active layers for parvoviruses in different filter membranes and thus to correlate the retention of viruses with the structure- and material-based characteristics of a particular filter type. The direct insight into the filter will also facilitate to explain the differential behavior of viruses under the influence of filter fouling, depressurization events or product-specific conditions in the feedstream.

Taken together, the visualization of parvoviruses inside the filter membrane combined with measurements of the viral load reduction provide a complete picture of virus filtration, which will help to better understand the mechanisms underlying parvovirus retention during nanofiltration of biotherapeutic products.

CRediT authorship contribution statement

Remo Leisi: Conceptualization, Methodology, Validation, Formal analysis, Investigation, Writing - original draft, Writing - review & editing. **Jan Bieri:** Methodology, Investigation. **Nathan J. Roth:** Conceptualization, Writing - review & editing, Supervision. **Carlos Ros:** Conceptualization, Validation, Writing - review & editing, Supervision, Project administration.

Acknowledgement

We thank T. Nowak and T. Wiegand of CSL Behring, Marburg for providing materials and supporting us with their expertise in virus filtration. We also thank U. Kämpfer of the mass spectrometry service at the University of Bern for his technical support.

Appendix A. Supplementary data

Supplementary data to this article can be found online at https://doi.org/10.1016/j.memsci.2020.118012.

References

[1] M.M. Lieber, R.E. Benveniste, D.M. Livingston, G.J. Todaro, Mammalian cells in culture frequently release type C viruses, Science 182 (1973) 56–59, https://doi.org/10.1126/science.182.4107.56 (80-.).

[2] N.J. Roth, Pathogen reduction of blood components and plasma derivatives, in: T. L. Simon, J. McCullough, E.L. Snyder, B.G. Solheim, R.G. Strauss (Eds.), Ross. Princ. Transfus. Med., John Willey & Sons, 2016, pp. 632–641.
[3] R. Cameron, K. Smith, Virus clearance methods applied in bioprocessing operations: an overview of selected inactivation and removal methods, Pharm. Bioprocess. 2 (2014) 75–83, https://doi.org/10.4155/pbp.13.61.
[4] A. Gröner, C. Broumis, R. Fang, T. Nowak, B. Popp, W. Schäfer, N.J. Roth, Effective inactivation of a wide range of viruses by pasteurization, Transfusion 58 (2018) 41–51, https://doi.org/10.1111/trf.14390.
[5] S. Caballero, J.M. Diez, F.J. Belda, M. Otegui, S. Herring, N.J. Roth, D. Lee, R. Gajardo, J.I. Jorquera, Robustness of nanofiltration for increasing the viral safety margin of biological products, Biologicals 42 (2014) 79–85, https://doi.org/10.1016/j.biologicals.2013.10.003.
[6] R.L. Garnick, Raw materials as a source of contamination in large-scale cell culture, Dev. Biol. Stand. 93 (1998) 21–29.
[7] M. Moody, W. Alves, J. Varghese, F. Khan, Mouse minute virus (MMV) contamination - a case study: detection, root cause determination, and corrective actions, PDA J. Pharm. Sci. Technol. (2011) 580–588, https://doi.org/10.5731/pdajpst.2011.00824.
[8] E.D. Heegaard, K.E. Brown, Human parvovirus B19, Clin. Microbiol. Rev. 15 (2002) 485–505, https://doi.org/10.1128/CMR.15.3.485-505.2002.
[9] B. Kaufmann, A.A. Simpson, M.G. Rossmann, The structure of human parvovirus B19, Proc. Natl. Acad. Sci. U.S.A. 101 (2004) 11628–22633, https://doi.org/10.1073/pnas.0402992101.
[10] A.L. Llamas-Saiz, M. Agbandje-McKenna, W.R. Wikoff, J. Bratton, P. Tattersall, M. G. Rossmann, Structure determination of minute virus of mice, Acta Crystallogr. Sect. D Biol. Crystallogr. 53 (1997) 93–102, https://doi.org/10.1107/S0907444996010566.
[11] L. Govindasamy, K. Hueffer, C.R. Parrish, M. Agbandje-McKenna, Structures of host range-controlling regions of the capsids of canine and feline parvoviruses and mutants, J. Virol. 77 (2003) 12211–12221, https://doi.org/10.1128/jvi.77.22.12211-12221.2003.
[12] L.J. Harris, E. Skaletsky, A. McPherson, Crystallographic structure of an intact IgG1 monoclonal antibody, J. Mol. Biol. 275 (1998) 861–872, https://doi.org/10.1006/jmbi.1997.1508.
[13] R. Esfandiary, D.B. Hayes, A. Parupudi, J. Casas-Finet, S. Bai, H.S. Samra, A. U. Shah, H.A. Sathish, A systematic multitechnique approach for detection and characterization of reversible self-association during formulation development of therapeutic antibodies, J. Pharm. Sci. 102 (2013) 3089–3099, https://doi.org/10.1002/jps.23654.
[14] E. Gefroh, H. Dehghani, M. McClure, L. Connell-Crowley, G. Vedantham, Use of MMV as a single worst-case model virus in viral filter validation studies, PDA J. Pharm. Sci. Technol. 68 (2014) 297–311, https://doi.org/10.5731/pdajpst.2014.00978.
[15] T. Nowak, B. Popp, N.J. Roth, Choice of parvovirus model for validation studies influences the interpretation of the effectiveness of a virus filtration step, Biologicals 60 (2019) 85–92, https://doi.org/10.1016/j.biologicals.2019.04.003.
[16] T. Tsurumi, N. Osawa, T. Hirasaki, K. Yamaguchi, S.I. Manabe, T. Yamashiki, Mechanism of removing monodisperse gold particles from a suspension using cuprammonium regenerated cellulose hollow fiber (bmm hollow fiber), Polym. J. 22 (1990) 304–311, https://doi.org/10.1295/polymj.22.304.
[17] K. Yamaguchi, E. Miyagawa, H. Takahashi, T. Miyazaki, H. Ikeda, Electron microscopic estimation of removal of parvovirus B19 (HPVB19) by nanofiltration with a novel filter membrane, J. Membr. Sci. 298 (2007) 99–109, https://doi.org/10.1016/j.memsci.2007.04.009.
[18] H. Nazem-Bokaee, F. Fallahianbijan, D. Chen, S.M. O'Donnell, C. Carbrello, S. Giglia, D. Bell, A.L. Zydney, Probing pore structure of virus filters using scanning electron microscopy with gold nanoparticles, J. Membr. Sci. 552 (2018) 144–152, https://doi.org/10.1016/j.memsci.2018.01.069.
[19] F. Fallahianbijan, S. Giglia, C. Carbrello, A.L. Zydney, Use of fluorescently-labeled nanoparticles to study pore morphology and virus capture in virus filtration membranes, J. Membr. Sci. 536 (2017) 52–58, https://doi.org/10.1016/j.memsci.2017.04.066.
[20] P. Kosiol, B. Hansmann, M. Ulbricht, V. Thom, Determination of pore size distributions of virus filtration membranes using gold nanoparticles and their correlation with virus retention, J. Membr. Sci. 533 (2017) 289–301, https://doi.org/10.1016/j.memsci.2017.03.043.
[21] P. Kosiol, M.T. Müller, B. Schneider, B. Hansmann, V. Thom, M. Ulbricht, Determination of pore size gradients of virus filtration membranes using gold nanoparticles and their relation to fouling with protein containing feed streams, J. Membr. Sci. 548 (2018) 598–608, https://doi.org/10.1016/j.memsci.2017.11.048.
[22] M. Bakhshayeshi, N. Jackson, R. Kuriyel, A. Mehta, R. van Reis, A.L. Zydney, Use of confocal scanning laser microscopy to study virus retention during virus filtration, J. Membr. Sci. 379 (2011) 260–267, https://doi.org/10.1016/j.memsci.2011.05.069.
[23] S.K. Dishari, A. Venkiteshwaran, A.L. Zydney, Probing effects of pressure release on virus capture during virus filtration using confocal microscopy, Biotechnol. Bioeng. 112 (2015) 2115–2122, https://doi.org/10.1002/bit.25614.
[24] N.B. Jackson, M. Bakhshayeshi, A.L. Zydney, A. Mehta, R. van Reis, R. Kuriyel, Internal virus polarization model for virus retention by the Ultipor® VF Grade DV20 membrane, Biotechnol. Prog. 30 (2014) 856–863, https://doi.org/10.1002/btpr.1897.
[25] H. Nazem-Bokaee, D. Chen, S.M. O'Donnell, A.L. Zydney, New insights into the performance characteristics of the Planova-series hollow-fiber parvovirus filters using confocal and electron microscopy, Biotechnol. Bioeng. 116 (2019) 2010–2017, https://doi.org/10.1002/bit.26991.
[26] A. Slocum, M. Burnham, P. Genest, A. Venkiteshwaran, D. Chen, J. Hughes, Impact of virus preparation quality on parvovirus filter performance, Biotechnol. Bioeng. 110 (2013) 229–239, https://doi.org/10.1002/bit.24600.
[27] P. Kosiol, C. Kahrs, V. Thom, M. Ulbricht, B. Hansmann, Investigation of virus retention by size exclusion membranes under different flow regimes, Biotechnol. Prog. 35 (2019), https://doi.org/10.1002/btpr.2747.
[28] S.K. Dishari, M.R. Micklin, K.J. Sung, A.L. Zydney, A. Venkiteshwaran, J.N. Earley, Effects of solution conditions on virus retention by the Viresolve® NFP filter, Biotechnol. Prog. 31 (2015) 1280–1286, https://doi.org/10.1002/btpr.2125.
[29] D. Strauss, J. Goldstein, T. Hongo-Hirasaki, Y. Yokoyama, N. Hirotomi, T. Miyabayashi, D. Vacante, Characterizing the impact of pressure on virus filtration processes and establishing design spaces to ensure effective parvovirus removal, Biotechnol. Prog. 33 (2017) 1294–1302, https://doi.org/10.1002/btpr.2506.
[30] J. Adan-Kubo, M. Tsujikawa, K. Takahashi, T. Hongo-Hirasaki, K. Sakai, Microscopic visualization of virus removal by dedicated filters used in biopharmaceutical processing: impact of membrane structure and localization of captured virus particles, Biotechnol. Prog. 35 (2019), https://doi.org/10.1002/btpr.2875.
[31] T. Hongo-Hirasaki, K. Yamaguchi, K. Yanagida, H. Hayashida, S. Ide, Effects of varying virus-spiking conditions on a virus-removal filter Planova™ 20N in a virus validation study of antibody solutions, Biotechnol. Prog. 27 (2011) 162–169, https://doi.org/10.1002/btpr.533.
[32] N. Previsani, S. Fontana, B. Hirt, P. Beard, Growth of the parvovirus minute virus of mice MVMp3 in EL4 lymphocytes is restricted after cell entry and before viral DNA amplification: cell- specific differences in virus uncoating in vitro, J. Virol. 71 (1997) 7769–7780.
[33] M. Cabatingan, Impact of virus stock quality on virus filter validation, Bioprocess Int. 3 (2005) 39–43.
[34] S.F. Cotmore, S. Hafenstein, P. Tattersall, Depletion of virion-associated divalent cations induces parvovirus minute virus of mice to eject its genome in a 3'-to-5' direction from an otherwise intact viral particle, J. Virol. 84 (2010) 1945–1956, https://doi.org/10.1128/jvi.01563-09.
[35] R. Leisi, M. Von Nordheim, C. Ros, C. Kempf, The VP1u receptor restricts parvovirus B19 uptake to permissive erythroid cells, Viruses 8 (2016), https://doi.org/10.3390/v8100265.
[36] B. Mani, C. Baltzer, N. Valle, J.M. Almendral, C. Kempf, C. Ros, Low pH-dependent endosomal processing of the incoming parvovirus minute virus of mice virion leads to externalization of the VP1 N-terminal sequence (N-VP1), N-VP2 cleavage, and uncoating of the full-length genome, J. Virol. 80 (2006) 1015–1024, https://doi.org/10.1128/jvi.80.2.1015-1024.2006.
[37] M.J. Merchlinsky, P.J. Tattersall, J.J. Leary, S.F. Cotmore, E.M. Gardiner, D. C. Ward, Construction of an infectious molecular clone of the autonomous parvovirus minute virus of mice, J. Virol. 47 (1983) 227–232.
[38] P. Tattersall, P.J. Cawte, A.J. Shatkin, D.C. Ward, Three structural polypeptides coded for by minite virus of mice, a parvovirus, J. Virol. 20 (1976) 273–289.
[39] R. Wolfisberg, C. Kempf, C. Ros, Late maturation steps preceding selective nuclear export and egress of progeny parvovirus, J. Virol. 90 (2016) 5462–5474, https://doi.org/10.1128/jvi.02967-15.
[40] P. Plevka, K. Tars, L. Liljas, Structure and stability of icosahedral particles of a covalent coat protein dimer of bacteriophage MS2, Protein Sci. 18 (2009) 1653–1661, https://doi.org/10.1002/pro.184.
[41] E.D. Horowitz, K.S. Rahman, B.D. Bower, D.J. Dismuke, M.R. Falvo, J.D. Griffith, S. C. Harvey, A. Asokan, Biophysical and ultrastructural characterization of adeno-associated virus capsid uncoating and genome release, J. Virol. 87 (2013) 2994–3002, https://doi.org/10.1128/jvi.03017-12.
[42] R.P. Haugland, Coupling of monoclonal antibodies with fluorophores, Methods Mol. Biol. 45 (1995) 205–221, https://doi.org/10.1385/0-89603-308-2:205.
[43] J.E. Berlier, A. Rothe, G. Buller, J. Bradford, D.R. Gray, B.J. Filanoski, W. G. Telford, S. Yue, J. Liu, C.Y. Cheung, W. Chang, J.D. Hirsch, J.M. Beechem, R. P. Haugland, R.P. Haugland, Quantitative comparison of long-wavelength Alexa fluor dyes to cy dyes: fluorescence of the dyes and their bioconjugates, J. Histochem. Cytochem. 51 (2003) 1699–1712, https://doi.org/10.1177/002215540305101214.
[44] C.A. Schneider, W.S. Rasband, K.W. Eliceiri, NIH Image to ImageJ: 25 years of image analysis, Nat. Methods 9 (2012) 671–675, https://doi.org/10.1038/nmeth.2089.
[45] M. Tsujikawa, Y. Ohkubo, M. Masuda, H. Tanaka, K. Takahashi, Y. Sasaki, M. Yunoki, K. Ikuta, Caution in evaluation of removal of virus by filtration: misinterpretation due to detection of viral genome fragments by PCR, J. Virol. Methods. 178 (2011) 39–43, https://doi.org/10.1016/j.jviromet.2011.08.009.
[46] S. Ideno, K. Takahashi, K. Yusa, K. Sakai, Quantitative PCR evaluation of parvovirus B19 removal via nanofiltration, J. Virol. Methods. 275 (2020), https://doi.org/10.1016/j.jviromet.2019.113755.
[47] S. Lute, M. Bailey, J. Combs, M. Sukumar, K. Brorson, Phage passage after extended processing in small-virus-retentive filters, Biotechnol. Appl. Biochem. 47 (2007) 141, https://doi.org/10.1042/ba20060254.
[48] D.R. Asher, A.L. Slocum, K.F. Bergmann, P. Genest, A.B. Katz, J.J. Morais, C. M. Lawrence, P. Greenhalgh, Predicting virus filtration performance with virus spike characterization, Bioprocess Int. 9 (2011) 26–36.
[49] N.Z. Khan, J.J. Parrella, P.W. Genest, M.S. Colman, Filter preconditioning enables representative scaled-down modelling of filter capacity and viral clearance by mitigating the impact of virus spike impurities, Biotechnol. Appl. Biochem. 52 (2009) 293, https://doi.org/10.1042/ba20080133.

[50] P. De Vilmorin, A. Slocum, T. Jaber, O. Schaefer, H. Ruppach, P. Genest, Achieving a successful scale-down model and optimized economics through parvovirus filter validation using purified TrueSpikeTM viruses, PDA J. Pharm. Sci. Technol. 69 (2015) 440–449, https://doi.org/10.5731/pdajpst.2015.01054.

[51] A. Furiga, G. Pierre, M. Glories, P. Aimar, C. Roques, C. Causserand, M. Berge, Effects of ionic strength on bacteriophage MS2 behavior and their implications for the assessment of virus retention by ultrafiltration membranes, Appl. Environ. Microbiol. 77 (2011) 229–236, https://doi.org/10.1128/AEM.01075-10.

[52] R. Golmohammadi, K. Valegård, K. Fridborg, L. Liljas, The refined structure of bacteriophage MS2 at 2·8 Å resolution, J. Mol. Biol. 234 (1993) 620–639, https://doi.org/10.1006/jmbi.1993.1616.

[53] ATTO-TEC Germany, Prod. Inf. Atto NHS-Esters (2019), in: https://www.atto-tec.com/images/ATTO/Procedures/NHS.pdf. (Accessed 28 November 2019).

[54] S. Lute, W. Riordan, L.F. Pease, D.H. Tsai, R. Levy, M. Haque, J. Martin, I. Moroe, T. Sato, M. Morgan, M. Krishnan, J. Campbell, P. Genest, S. Dolan, K. Tarrach, A. Meyer, H. Aranha, M. Bailey, J. Bender, J. Carter, Q. Chen, C. Dowd, R. Jani, D. Jen, S. Kidd, T. Meltzer, K. Remington, I. Rice, C. Romero, T. Sato, M. Jornitz, C. M. Sekura, G. Sofer, R. Specht, K. Tarrach, P. Wojciechowski, M.R. Zachariah, M. J. Tarlov, M. Etzel, K. Brorson, A consensus rating method for small virus-retentive filters. I. Method development, PDA J. Pharm. Sci. Technol. 62 (2008) 318–333.

[55] C. Ros, C. Baltzer, B. Mani, C. Kempf, Parvovirus uncoating in vitro reveals a mechanism of DNA release without capsid disassembly and striking differences in encapsidated DNA stability, Virology 345 (2006) 137–147, https://doi.org/10.1016/j.virol.2005.09.030.

[56] C. Ros, M. Gerber, C. Kempf, Conformational changes in the VP1-unique region of native human parvovirus B19 lead to exposure of internal sequences that play a role in virus neutralization and infectivity, J. Virol. 80 (2006) 12017–12024, https://doi.org/10.1128/jvi.01435-06.